Applied Catalysis B: Environmental 163 (2015) 306–312

Contents lists available at ScienceDirect

Applied Catalysis B: Environmental

journal homepage: www.elsevier.com/locate/apcatb

Efficient catalytic removal of formaldehyde at room temperature using AlOOH nanoflakes with deposited Pt

Zhihua Xu[a,b,c], Jiaguo Yu[a,*], Mietek Jaroniec[b,**]

[a] State Key Laboratory of Advanced Technology for Materials Synthesis, Processing, Wuhan University of Technology, Wuhan 430070, PR China
[b] Department of Chemistry and Biochemistry, Kent State University, Kent, OH 44242, USA
[c] Hubei Key Laboratory for Processing and Application of Catalytic Materials, Huanggang Normal University, Huanggang 438000, PR China

ARTICLE INFO

Article history:
Received 5 May 2014
Received in revised form 7 July 2014
Accepted 8 August 2014
Available online 17 August 2014

Keywords:
Aluminum oxyhydroxide
Pt/AlOOH
Adsorption
Formaldehyde removal
Catalytic decomposition

ABSTRACT

Mesoporous AlOOH with deposited Pt (Pt/AlOOH) catalyst was prepared by combining the microemulsion-assisted synthesis of AlOOH nanoflakes with $NaBH_4$-reduction of Pt precursor, and exhibited a remarkable catalytic activity as well as stability for elimination of formaldehyde (HCHO) vapor at room temperature. As compared to Pt deposited on calcined AlOOH (Pt/AlOOH-c), Pt on a commercial Al_2O_3 (Pt/c-Al_2O_3) and Pt on P25 (Pt/TiO_2), the Pt/AlOOH nanoflakes showed the highest catalytic activity toward decomposition of HCHO at room temperature. The excellent performance of Pt/AlOOH nanoflakes could be attributed to the abundance of surface hydroxyls, high dispersion of Pt nanoparticles, excellent adsorption performance of AlOOH, and its high specific surface area and large pore volume. The mechanism of HCHO decomposition was investigated with respect to the behavior of adsorbed intermediates on Pt/AlOOH surface at room temperature using in situ DRIFTS. The result suggests that surface formate is the main reaction intermediate during the HCHO oxidation and it could be directly oxidized to CO_2 in the presence of O_2. By taking advantage of high adsorption affinity of AlOOH nanoflakes and excellent catalytic activity of Pt nanoparticles toward HCHO it was possible to design a superior nanostructured catalyst for room temperature decomposition of HCHO. This strategy can be also used to fabricate novel nanostructured catalysts for advanced applications such as environmental remediation.

1. Introduction

Formaldehyde (HCHO) is considered as a major indoor air pollutant, which can cause serious health problems [1–3]. Considerable efforts have been made to eliminate HCHO from air in order to meet the strict environmental regulations [3–10]. Room-temperature HCHO oxidation over supported noble metals (like Pt, Pd and Au) is an effective and promising technology for reducing the HCHO concentration in atmosphere due to its simple operation, low energy demand and complete conversion of toxic HCHO into CO_2 and water [11–13]. Various metal oxides including TiO_2 [11,12], MnO_2 [14], Fe_2O_3 [15], Al_2O_3 [16,17], ZrO_2, MgO [18], In_2O_3 [19], CeO_2 and Co_3O_4 [20,21] and the composites like MnO_x–CeO_2 [22] and Co_3O_4–CeO_2 [13], as well as non-metal oxides like SiO_2 [23] have been investigated as solid supports for noble metal catalysts used for complete decomposition of formaldehyde at room (or ambient) temperature. The aforementioned supports can greatly promote the activity of the deposited noble metal catalysts due to their high dispersion and electronic structure alteration, redox properties of the supports and/or synergistic interaction with the noble metal catalyst and support. Currently, the development of efficient and feasible materials for HCHO removal from air is still an interesting and incompletely solved problem.

Recently, mesoporous nanostructures with designed surface functionality and unique morphology have attracted a widespread attention because of their potential applications in catalysis, adsorption, separations, controlled drug delivery and biosensing [24–32]. Among mesoporous materials, the nanostructured AlOOH, due to its low cost, environmental friendliness and easy processing has gained a lot of attention because of its high surface affinity and tunable morphological and structural features such as shape, specific surface area and pore/particle size. As a result, AlOOH materials with novel morphological and structural features have been extensively explored to enhance its performance in a wide range of potential applications [32–38]. For example, hierarchical boehmite was shown to be a very effective sorbent for removal of Congo red, phenol and Cr(VI) from model wastewater [39,40]. However, to the

* Corresponding author. Tel.: +86 27 87871029; fax: +86 27 87879468.
** Corresponding author. Tel.: +1 330 672 3790; fax: +1 330 672 3816.
E-mail addresses: jiaguoyu@yahoo.com (J. Yu), jaroniec@kent.edu (M. Jaroniec).

http://dx.doi.org/10.1016/j.apcatb.2014.08.017
0926-3373/

best of our knowledge, AlOOH with high surface area and strong affinity has not yet been investigated as a support for Pt nanoparticles for complete oxidation of gaseous HCHO at room temperature.

It is generally accepted that a good support should influence the nature of the active component and subsequently, its catalytic activity by affecting the formation, distribution and dispersion of the active component on the support surface [41]. In our previous work [42], we showed that the microemulsion-assisted synthesis afforded AlOOH with abundance of hydroxyl groups, which was shown to be a very effective adsorbent for HCHO. Herein, we report the synthesis of AlOOH nanoflakes with deposited Pt, which exhibit respectively both high adsorption affinity (AlOOH nanoflakes) and high catalytic activity (highly dispersed Pt nanoparticles) toward adsorption and catalytic degradation of HCHO at room temperature. As compared to the reported Al_2O_3 support [16,17], the as-made AlOOH nanoflakes are expected to promote the performance of the aforementioned nanostructured catalyst toward degradation of HCHO due to the following aspects: (1) AlOOH with nanoflake-type morphology possesses a plenty of hydroxyl groups, unique porosity and high surface area that enhance HCHO adsorption; (2) high specific surface area of AlOOH assures high dispersion of noble metal, resulting in large concentration of catalytically active sites; and (3) enhanced adsorption of HCHO on AlOOH nanoflakes increases concentration of HCHO molecules in the proximity of Pt nanoparticles, facilitating catalytic decomposition of HCHO into CO_2 and H_2O.

2. Experimental

2.1. Preparation of AlOOH and Pt/AlOOH catalyst

AlOOH was synthesized as follows: a mixture containing 100 mL of cyclohexane and 20.46 g of polyethyleneglycol (PEG 400) was magnetically stirred and heated to 50 °C. After stirring for 10 min at 50 °C, 20 mL of $Al(NO_3)_3$ solution (0.32 M) and 3.50 g of NH_3 solution (27 wt%) were added stepwise to the above mixture, and then aged for 8 h to allow precipitation of aluminum oxyhydroxide. At the end of the synthesis, about 30 mL of isopropanol was added to the mixture to destabilize the microemulsion structure. The resulting mixture was separated by centrifugation and the powder was collected after washing with deionized water (four times) and ethanol (two times) and drying at ca. 65 °C overnight under vacuum and at 80 °C for ca. 30 min. For the purpose of comparison, the as-prepared AlOOH powder was calcined at 450 °C for 2 h at a heating rate of 2 °C min^{-1}, and the resulting powder was denoted as AlOOH-c.

AlOOH-supported Pt catalyst (Pt/AlOOH) was obtained by adding 0.4 g of the as-prepared AlOOH into an H_2PtCl_6 solution under magnetic stirring (the nominal weight of Pt was 0.8 wt%). After impregnation for 20 min, 5 mL of the mixed solution of $NaBH_4$ (0.1 mol/L) and NaOH (0.1 mol/L) was quickly added into the suspension under vigorous stirring for 30 min, and then the suspension was evaporated at 80 °C under stirring. Finally, the resulting powder was continuously dried overnight at 80 °C. For the purpose of comparison, the same nominal weight of Pt was introduced into commercial Al_2O_3 (denoted as Pt/c-Al_2O_3), AlOOH-c (denoted as Pt/AlOOH-c) and over P25 (denoted as Pt/TiO_2).

2.2. Characterization

X-ray diffraction (XRD) measurements were performed using a Philips X'Pert powder X-ray diffractometer with Cu Kα radiation (λ = 0.15419 nm). Transmission electron microscopy (TEM) images were obtained with a JEM-2100F electron microscope (JEOL, Japan). X-ray photoelectron spectroscopy (XPS) measurements were performed on a Kratos XSAM800 XPS system with Al Kα source and a charge neutralizer, and all the binding energies were referenced to the C 1s peak at 284.8 eV of the surface adventitious carbon. Nitrogen adsorption–desorption isotherms were obtained on an ASAP 2020 (Micromeritics Instrument, USA). All samples were degassed in vacuum at 100 °C prior to adsorption measurements. The Brunauer–Emmett–Teller (BET) surface area (S_{BET}) was determined by a multipoint BET method using adsorption data in the relative pressure P/P_0 range of 0.05–0.2. The single-point pore volume (V_p) was estimated from the amount adsorbed at a relative pressure of 0.98. The pore size distributions (PSD) were calculated using adsorption branches of nitrogen adsorption–desorption isotherms by the improved KJS method [37,43]. Fourier transform infrared spectra (FTIR) were collected using a Shimadzu IRAffinity-1 FTIR spectrometer in the frequency range of 4000–400 cm^{-1}. In situ diffuse reflectance infrared Fourier transform spectra (DRIFTS) were recorded in Thermo Fisher 6700. The catalysts were pretreated in a dried air gas flow at 150 °C for 1 h in an in situ cell reactor, and then the reactant gas mixture (78 ppm HCHO + O_2) was introduced into the DRIFT cell at room temperature via separate mass flow meters at flow rates of 30 mL min^{-1}. All spectra were measured with a resolution of 4 cm^{-1}. A background spectrum was subtracted from each spectrum. Hydrogen temperature programmed reduction (H_2-TPR) and metal dispersion were performed on the BELCAT-B (Japan) instrument. In each experiment, 60 mg of the sample was loaded into the U-type quartz tube. Prior H_2-TPR experiment, the sample was pretreated in He (50 mL min^{-1}) at 200 °C for 1 h and then the temperature was ramped from room temperature to 550 °C at 10 °C min^{-1} with introducing the reducing gas (10% H_2/Ar) at a flow rate of 30 mL min^{-1}. Measurement of the metal dispersion by CO pulse chemisorption was carried out at room temperature by a pulse injection method. The samples were first reduced under pure hydrogen (50 mL min^{-1}) at 200 °C for 1 h and further outgassed under He (50 mL min^{-1}) for 0.5 h at the same temperature. Subsequently, CO pluses were injected into the carrier gas intermittently after the sample was cooled to room temperature, and the whole process was detected by a TCD.

2.3. Adsorption and catalytic activity tests

The room temperature adsorption and catalytic oxidation of HCHO were performed in an organic glass reactor with a volume of 6 L covered by a layer of aluminum foil on its inner wall. 0.1 g of the as-prepared sample was dispersed in 5 mL of water under stirring. Then, the suspension was coated on the bottom of glass petri dish having diameter of 14 cm and dried in an oven at 80 °C for 1 h. After placing the sample-coated dish in the bottom of reactor with a glass slide cover, a certain amount of condensed HCHO (38%) was injected into the reactor having a 5 W fan at the bottom of the reactor. After 1–2 h, the HCHO solution was volatilized completely and the concentration of HCHO was stabilized. The analysis of HCHO, CO_2, CO and water vapor was conducted online with a Photoacoustic IR Multigas Monitor (INNOVA air Tech Instruments Model 1412). The HCHO vapor was allowed to reach adsorption equilibrium within the reactor prior to the experiment. The relative humidity was 25% and the adsorption time or catalytic oxidation time was 51 min. The initial concentration of HCHO after adsorption equilibrium was controlled at ca. 127 for adsorption test and ca. 139 ppm for catalytic oxidation test. All the adsorption and catalytic oxidation tests were carried out at room temperature and the relative humidity was near 25% RH, as well as the test time was 51 min. During the catalytic oxidation reaction, carbon dioxide concentration increased and HCHO concentration decreased steadily with time. The HCHO concentration decrease and CO_2 concentration increase (ppm, ΔCO_2, which is the difference between CO_2 concentrations at t reaction time

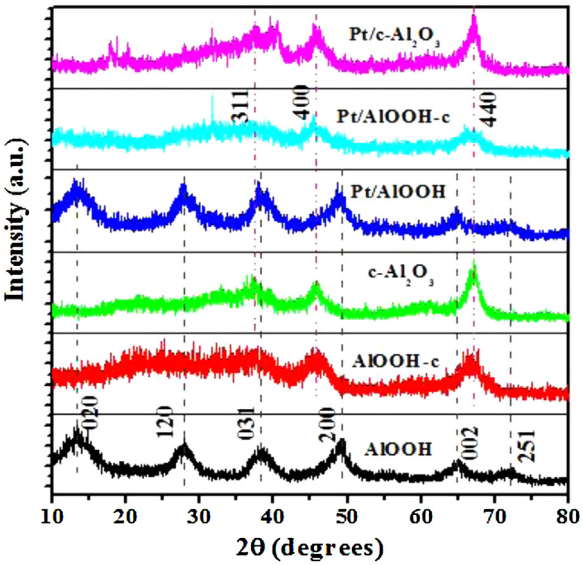

Fig. 1. XRD patterns of Pt/AlOOH, Pt/AlOOH-c, Pt/c-Al_2O_3, AlOOH (data taken from ref [42]), AlOOH-c and c-Al_2O_3.

Table 1
Pt dispersion and HCHO turnover frequency (TOF) at room temperature.

Catalysts	Pt dispersion (%)	TOF (min^{-1})
Pt/AlOOH	24.9	0.70
Pt/AlOOH-c	20.3	0.69
Pt/c-Al_2O_3	16.9	0.85
Pt/TiO_2	17.9	0.65

Table 2
Properties of the adsorbents and catalysts studied.

Samples	CR (%)	RC (ppm/g)	S_{BET} (m^2/g)	d_p (nm)	V_p (cm^3/g)
Pt/AlOOH	92	1278	282	4.1	0.27
AlOOH	46	577	488[a]	8.0[a]	0.85[a]
Pt/AlOOH-c	75	1028	322	6.3	0.47
AlOOH-c	48	615	419	10.6	1.14
Pt/c-Al_2O_3	76	1063	87	4.7	0.13
c-Al_2O_3	28	360	406	4.9	0.59
AlOOH*	23	290	310[a]	3.1[a]	0.28[a]
Pt/TiO_2	63	860	35	30.3, 52.1	0.16

CR, conversion of HCHO; RC, HCHO removal per the weight of the adsorbent or catalyst; S_{BET}, BET specific surface area; V_p, single-point pore volume; and d_p, pore width at the maximum of the pore size distribution.
[a] Data taken from ref [42].

and initial time) were used to evaluate the adsorption and/or catalytic performance. In the recycling experiments, the catalysts were just placed in a desiccator before the next run of HCHO oxidation.

The removal of HCHO was determined by the following equation:

$$\text{HCHO removal}\,(\%) = \frac{[\text{HCHO}]_I - [\text{HCHO}]_F}{[\text{HCHO}]_I} \times 100\%$$

where $[HCHO]_I$ (ppm) is the initial equilibrium concentration of HCHO before test, and $[HCHO]_F$ (ppm) is the final concentration of HCHO at the termination of the test.

3. Results and discussion

The XRD patterns of all the samples are shown in Fig. 1. The typical peaks of the as-prepared AlOOH can be clearly identified as orthorhombic γ-AlOOH (JCPDS No. 21-1307), and no peaks for other phases were observed, suggesting its relatively high purity. The diffraction peaks of AlOOH-c and commercial Al_2O_3 could be assigned to γ-Al_2O_3 [44,45]. It indicates that the as-prepared γ-AlOOH was transformed to γ-Al_2O_3 by thermal transformation at 450 °C in air. The diffraction patterns of the Pt catalysts studied are similar to those of the corresponding supports, indicating that Pt did not affect the phase structure of the samples; and no related diffraction peaks of Pt were observed, mainly due to the low content of Pt and/or the high dispersion of Pt nanoparticles.

Fig. 2 shows the TEM images of Pt/AlOOH, Pt/AlOOH-c and Pt/c-Al_2O_3. The supports of AlOOH (Fig. 2d) and AlOOH-c (Fig. 2e) consisted of agglomerated nanoflakes, indicating that the well-defined nanoflake structure of the as-prepared AlOOH was preserved during its calcination. The TEM image of commercial Al_2O_3 (c-Al_2O_3) shows that this material consisted of agglomerated nanoparticles (inset of Fig. 2c). As can be seen from TEM images Pt nanoparticles deposited on the surface of the supports studied are very small in size (3–4 nm). A detailed analysis indicated that Pt/AlOOH showed higher dispersion of Pt than Pt/AlOOH-c or Pt/c-Al_2O_3, which was also confirmed by the measured Pt dispersion (see data in Table 1). The higher Pt dispersion in the former system can be attributed to the nanoflake-type morphology and the presence of surface hydroxyls [17]. The morphology and microstructure of the supports influence the dispersion of noble metals on their surfaces, and presumably the subsequent catalytic activity.

The porous structure and texture of the samples were investigated by N_2 sorption analysis. Fig. 3 shows the nitrogen adsorption–desorption isotherms and the corresponding pore-size distribution curves (inset) for Pt/AlOOH, Pt/AlOOH-c and Pt/c-Al_2O_3. All isotherms are type IV with a type H2 hysteresis loop [46], indicating the presence of interconnected mesopores [47]. A comparison of Pt/c-Al_2O_3, Pt/AlOOH, and Pt/AlOOH-c shows a visible increase in the amount of adsorbed N_2 at high relative pressures between 0.5 and 1.0, especially for two latter samples, suggesting larger pore volumes for Pt/AlOOH and Pt/AlOOH-c. The reason for this behavior is that Pt/AlOOH and Pt/AlOOH-c consisted of a large amount of nanoflakes, which resulted in higher mesoporosity than that in the case of Pt/c-Al_2O_3. The pore-size distributions calculated for all the samples (inset of Fig. 3) are mainly in the range of 2.5–15 nm, further confirming the presence of mesopores. The pore structure parameters for all the samples including BET specific surface area (S_{BET}), pore volume (V_p) and pore width (d_p) at the maximum of PSD are listed in Table 2. As can be seen from Table 2 that all the Pt catalysts showed lower S_{BET}, V_p and d_p than the values obtained for the corresponding supports, which can be ascribed to the much larger density of Pt than that of the supports, and partial blocking of pores induced by usage of $NaBH_4$ and NaOH in the reduction process [11]. Pt/AlOOH-c exhibited the specific surface area of 322 m^2/g and the pore volume of 0.47 cm^3/g, larger than the values obtained for Pt/AlOOH (282 m^2/g and 0.27 cm^3/g); and Pt/c-Al_2O_3 showed the lowest S_{BET} and V_p (86 m^2/g and V_p 0.13 cm^3/g). In general, larger specific surface area and pore volume are favorable for dispersion of noble metals, and can provide more adsorption and/or reacting sites for HCHO, which results in higher catalytic activity.

Fig. 4 shows the FTIR spectra of Pt/AlOOH, Pt/AlOOH-c and Pt/c-Al_2O_3. A strong and broad band at ca. 3450 cm^{-1} and a moderate peak at ca. 1640 cm^{-1} in the spectra of all samples can be assigned to the stretching and bending vibrations of OH, respectively, indicating the presence of a large amount of hydroxyl groups on the surfaces of the samples studied. The sharp peak at ca. 1400 cm^{-1} in all spectra can be ascribed to the vibration overtone of surface OH groups [48] and/or the impurity of nitrate ions, and the bands between 780 and 500 cm^{-1} can be assigned to the vibration mode of AlO_6 [34,49]. Moreover, a shoulder peak ca. 3100 cm^{-1} and a sharp

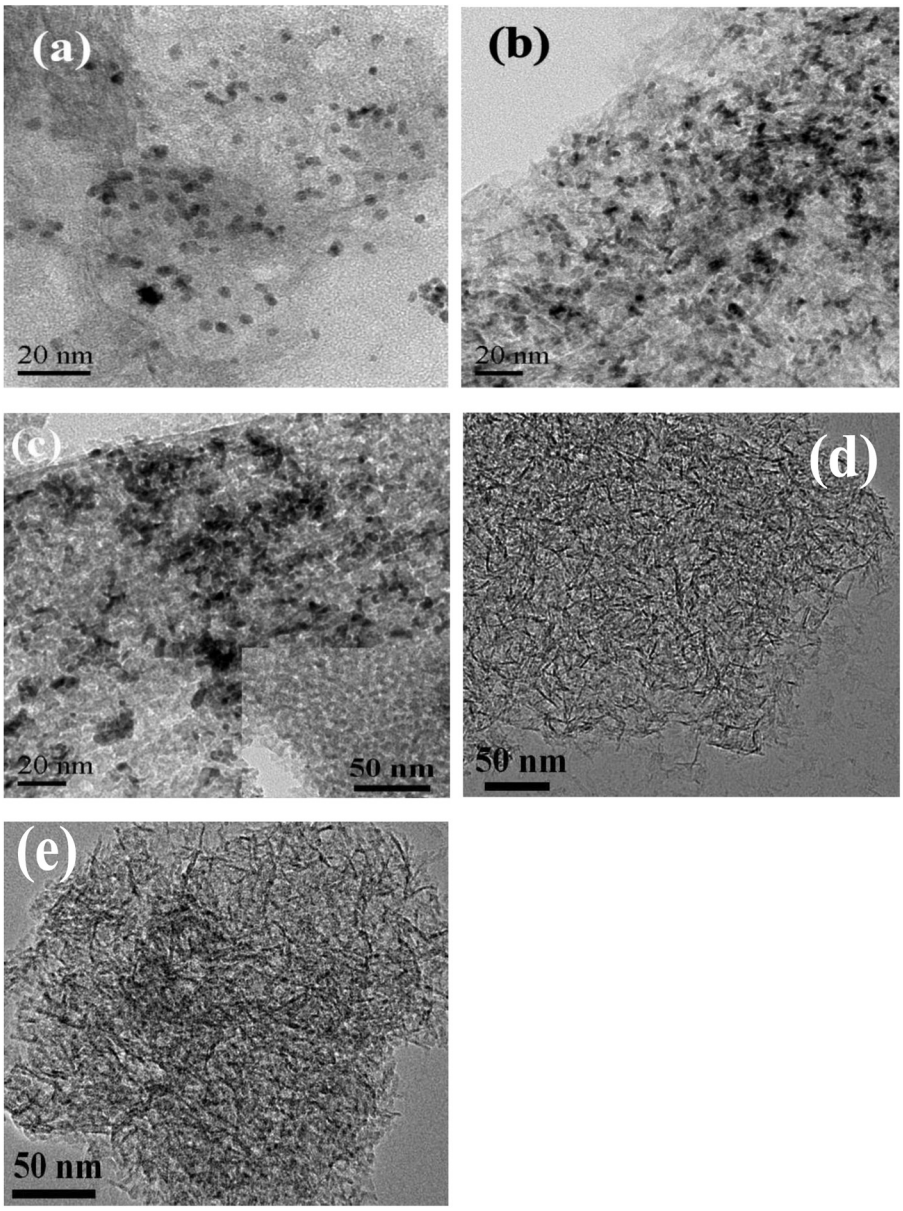

Fig. 2. TEM images of (a) Pt/AlOOH, (b) Pt/AlOOH-c and (c) Pt/c-Al_2O_3, and SEM images of (d) AlOOH and (e) AlOOH-c. Insets in panel (c) show the TEM image of c-Al_2O_3.

peak at ca. 1072 cm^{-1} in the spectrum of Pt/AlOOH can be attributed to the stretching and bending modes of (Al)—OH [35] respectively, further confirming that the support remains aluminum oxyhydroxide after loading of Pt nanoparticles.

The XPS measurements were carried out to quantitatively analyze the state and the content of Pt catalysts, and the molar ratio of oxygen in hydroxyl and total oxygen on the surface of the samples. Fig. 5 presents the Pt 4d and O 1s XPS spectra of Pt/AlOOH, Pt/AlOOH-c and Pt/c-Al_2O_3. The presence of Pt 4d at the binding energy of ca. 314.8 eV can be attributed to metallic Pt [50], further confirming the presence of Pt nanoparticles on the supports surfaces. The Pt content in all samples measured by XPS (shown in Table 3) are larger than the nominal bulk weight (0.8 wt%), indicating that Pt nanoparticles are mainly deposited on the surface of the catalysts. Moreover, Pt/AlOOH and Pt/AlOOH-c show the lower amounts of surface Pt than Pt/c-Al_2O_3. It can be rationalized by the larger pore volumes of AlOOH and AlOOH-c, which can facilitate incorporation of Pt nanoparticles into the interior of the supports. The deconvolution of the O 1s signal for all samples gives two peaks at 530.4–530.6 and 531.5–531.9 eV, which can be attributed to oxygen in the crystal structure ($O_{crystal}$) and hydroxyl (O_{OH}), respectively [51,52]. The ratio of O_{OH}/total O (O_{Total}) is listed in Table 3. Note that the ratio of O_{OH}/O_{Total} for Pt/AlOOH is larger than that of Pt/c-Al_2O_3, and Pt/AlOOH-c. This suggests that Pt/AlOOH possessed the largest amount of surface hydroxyls, which can promote its activity for the removal of HCHO [4,5].

Table 3
Results of XPS analysis of the as-synthesized samples.

Samples	Pt 4d (wt%)	OH/O_{Total}
Pt/AlOOH	1.3	47%
Pt/AlOOH-c	1.1	23%
Pt/c-Al_2O_3	2.4	32%

Fig. 6 compares the performance of HCHO removal on all the samples studied. HCHO concentrations on all the adsorbents decrease quickly within initial 5 min and then gradually level

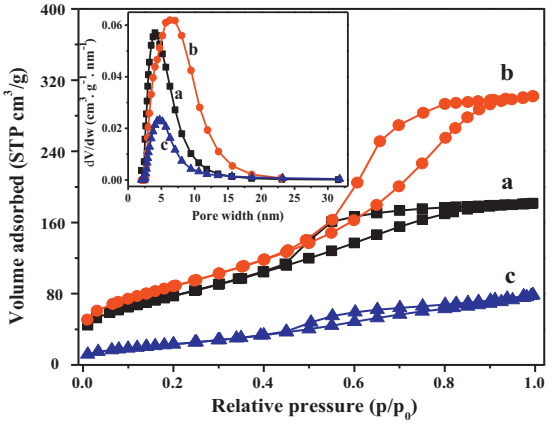

Fig. 3. Nitrogen adsorption/desorption isotherms and the corresponding pore size distributions (inset) for Pt/AlOOH (a), Pt/AlOOH-c (b) and Pt/c-Al_2O_3 (c).

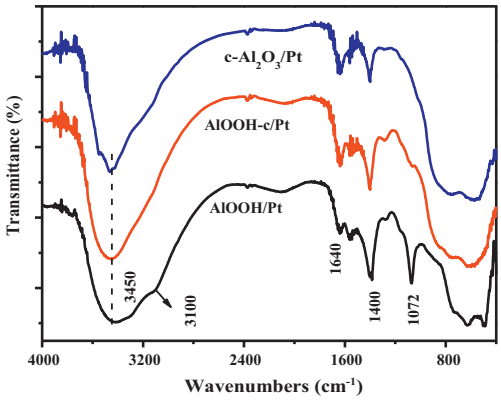

Fig. 4. FTIR spectra of Pt/AlOOH, Pt/AlOOH-c and Pt/c-Al_2O_3.

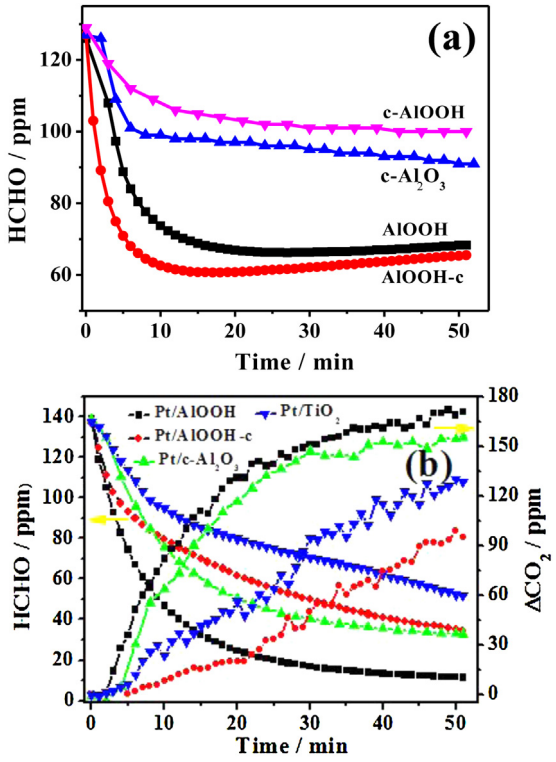

Fig. 6. (a) The concentration change of formaldehyde as a function of test time on AlOOH, AlOOH-c, AlOOH* and c-Al_2O_3 absorbents and (b) the concentration change of formaldehyde and ΔCO_2 as a function of reaction time for Pt/AlOOH, Pt/AlOOH-c, Pt/c-Al_2O_3 and Pt/TiO_2 catalysts.

off to approach the equilibrium (shown in Fig. 6a). For the purpose of comparison, the CO and CO_2 concentrations are almost unchanged in the whole process (not shown), indicating that HCHO is mainly physically adsorbed on AlOOH, AlOOH-c, commercial AlOOH (AlOOH*) and c-Al_2O_3. A slow increase in the HCHO concentration on AlOOH and AlOOH-c at the end of the test can be due to HCHO desorption from the adsorbent's surface. The weak interactions instead of the chemical bonding between HCHO molecule and adsorbents are presumably good for catalytic decomposition because HCHO molecules can be easily released from hydroxyl groups and make them available for adsorption again. It has been noted that the as-prepared AlOOH and AlOOH-c exhibited higher HCHO uptakes than those of AlOOH* and c-Al_2O_3, mainly due to the larger specific surface areas and pore volumes (listed in Table 2), as well as by the presence of surface hydroxyls.

As shown in Fig. 6b, the HCHO concentration decreases and CO_2 concentration increases, while the CO concentration is almost unchangeable (not shown) with increasing reaction time for all the catalysts, indicating the complete decomposition of HCHO at room temperature. A closer observation indicates that the HCHO concentration on Pt/AlOOH decreases much faster than that on Pt/AlOOH-c, Pt/c-Al_2O_3 and Pt/TiO_2; that is, the HCHO concentration after 51 min decreased from 139, 137, 139, 138 ppm to 11.2, 34.2, 32.7 and 52 ppm for Pt/AlOOH, Pt/AlOOH-c, Pt/c-Al_2O_3 and Pt/TiO_2, respectively. Accordingly, the CO_2 concentrations achieved

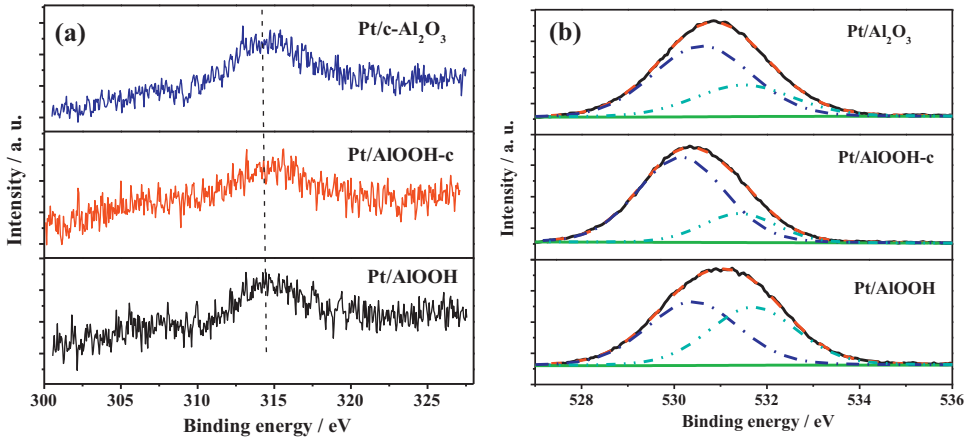

Fig. 5. Pt 4d (a) and O1s (b) XPS spectra of Pt/AlOOH, Pt/AlOOH-c and Pt/c-Al_2O_3.

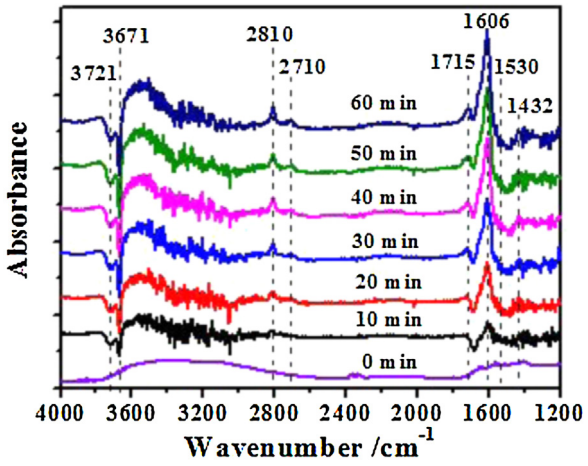

Fig. 7. Dynamic changes of in situ DRIFTS of the Pt/AlOOH catalyst as a function of time in a flow of O_2 + HCHO at room temperature.

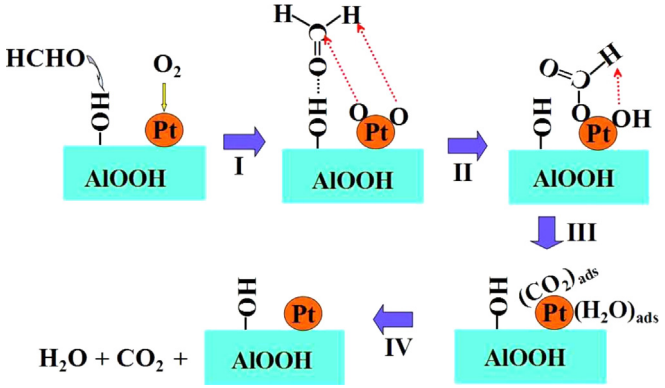

Fig. 8. A proposed reaction pathway for the complete oxidation of HCHO over the as-prepared Pt catalysts.

were ca. 171, 105, 157 and 129 ppm for Pt/AlOOH, Pt/AlOOH-c, Pt/c-Al_2O_3 and Pt/TiO_2, respectively. The above result indicates that Pt/AlOOH has a higher catalytic activity than Pt/AlOOH-c, Pt/c-Al_2O_3 and Pt/TiO_2 in HCHO oxidation at room temperature. In addition, the observed increase in the CO_2 concentration is larger than the decrease in the HCHO concentration, mainly due to desorption of some HCHO molecules from the reactor surface during experiment, and subsequent their oxidation to CO_2, as well as the measurement error of CO_2. The higher catalytic activity of Pt/AlOOH is due to the higher amount of surface hydroxyls and better adsorption performance of AlOOH, and the larger specific surface area and pore volume. Moreover, Pt/AlOOH-c showed a similar decrease in the HCHO concentration as that recorded for Pt/c-Al_2O_3, while much lower increase in ΔCO_2 concentration. The former behavior is mainly due to the better adsorption performance of AlOOH-c and larger surface area and pore volume, while the latter behavior is due to the lower Pt loading and smaller amount of surface hydroxyls. Moreover, the calculated TOF for catalytic decomposition of HCHO on Pt/AlOOH was 0.7 min^{-1} (Table 1), similar to that on Pt/AlOOH-c (0.69 min^{-1}) and Pt/TiO_2 (0.65 min^{-1}), and smaller than that on Pt/c-Al_2O_3 (0.85 min^{-1}). These data suggest that the better performance of Pt/AlOOH for removal of HCHO is presumably due to the higher adsorption affinity of AlOOH nanoflakes toward HCHO.

Fig. 7 shows the changes in the DRIFTS spectra of Pt/AlOOH catalyst as a function of time in a flow of HCHO + O_2 at room temperature. After the catalyst was exposed to the gaseous mixture of HCHO + O_2 at room temperature, the bands at 3721, 3671, 2810, 2710, 1715, 1606, 1530 and 1432 cm^{-1} appeared. With time increasing, the intensities of bands increased and reached a steady level after ca. 40 min. According to previous reports, two bands at ca. 1716 and 1606 cm^{-1} were attributed to the vibration of formate [53–55]. The small bands at ca. 2810 and 2710 cm^{-1} were assigned to the vibration of C—H, and the bands at ca. 3721 and 3671 cm^{-1} were attributed to isolated OH group of formic acid [54] and OH group bonded to the surface of the catalyst, respectively. However, there is no peak attributed to the molecularly adsorbed HCHO on the catalyst in the flow of HCHO + O_2 at room temperature. These DRIFTS spectra indicate that the adsorbed HCHO rapidly converts to formate species on the Pt/AlOOH catalyst. Moreover, a shoulder band at ca. 1530 and small band at ca. 1432 cm^{-1} in the spectra were due to carbonate species [54], originating from the formate species oxidation over the catalyst.

Apart from the direct adsorption and oxidation of HCHO on Pt active sites, a possible mechanism of the hydroxyl-assisted Pt catalytic oxidation of HCHO is proposed (as shown in Fig. 8) based on the in situ DRIFTS result and previously reported data [17,53]. HCHO is adsorbed on the surface hydroxyl [$(HCHO)_{ads}$] via hydrogen bonding [4,5], and O_2 is adsorbed and splits into active oxygen radicals on Pt surface [11]. One of the active oxygen radicals on Pt surface attacks the C atom, and then the other capture the H atom of the intermediate (step I). Then, the intermediate on the Pt surface quickly reconstructs into formate intermediate and active hydroxyl radical, and the occupied hydroxyl group is released (step II). The formate species were also reported by others as the main intermediates [56]. After that, the active hydroxyl radical adsorbed on Pt further oxidizes formate intermediate into adsorbed CO_2 $(CO_2)_{ads}$, and H_2O $(H_2O)_{ads}$ (step III). The adsorbed formate is presumably oxidized into CO_2, mainly because the concentration of CO with the reaction time in our experiment remained almost unchanged and no peak associated to molecularly adsorbed CO were observed in in situ DRIFTS spectra. Zhang et al. [53] also reported that abundance of hydroxyls facilitate the direct oxidation of formate species (HCOO-M + OH-M → H_2O + CO_2 + 2M, where M is Pt or Au). Finally, the adsorbed CO_2 and water desorb from the Pt surface, and Pt active sites are regenerated again (step IV). The surface hydroxyls of AlOOH are adsorption sites for HCHO, leading to a higher HCHO concentration in the vicinity of Pt and thereby facilitating the oxidation of HCHO. Thus, the surface hydroxyls of the support indirectly enhance activity of the catalyst. The larger amount of surface hydroxyls and Pt nanoparticles leads to higher activity of the catalyst toward oxidation of HCHO. Based on the above discussion, it is easy to understand that in the case of

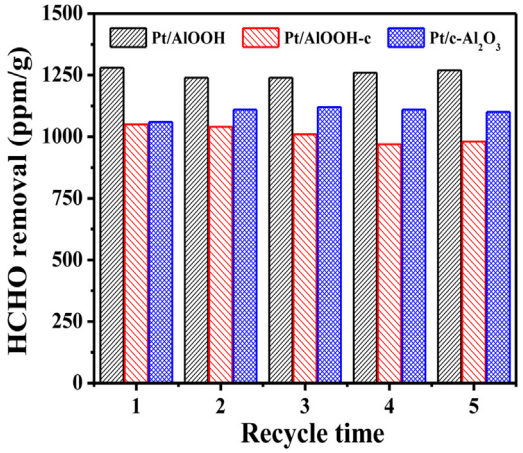

Fig. 9. Comparison of HCHO removal with recycle times over Pt/AlOOH, Pt/AlOOH-c and Pt/c-Al_2O_3.

Pt/AlOOH-c the increase in ΔCO_2 concentration at the same test time is small because of smaller amount of surface hydroxyls and Pt nanoparticles.

Stability of the catalyst is also a very important issue. To investigate the stability of the as-prepared samples in the complete decomposition of HCHO, the room-temperature oxidation was repeated five times over Pt/AlOOH, Pt/AlOOH-c and Pt/c-Al_2O_3 catalysts, and the results are presented in Fig. 9. The efficiencies of the HCHO degradation over Pt/AlOOH, Pt/AlOOH-c and Pt/c-Al_2O_3 for five repeated cycles did not change as compared to that obtained in the first-cycle, indicating that the as-prepared catalysts can maintain a stable and efficient catalytic performance. Furthermore, Pt/AlOOH exhibited higher catalytic activity toward HCHO decomposition as compared to Pt/AlOOH-c and Pt/c-Al_2O_3, further suggesting that it has potential to be an efficient catalyst for complete oxidation of HCHO at room temperature.

4. Conclusions

HCHO can be completely oxidized into CO_2 over Pt/AlOOH, Pt/AlOOH-c and Pt/c-Al_2O_3 catalysts at room temperature. Pt/AlOOH catalyst showed an excellent catalytic stability and higher HCHO oxidation activity than Pt/AlOOH-c and Pt/c-Al_2O_3, due to the larger amount of surface hydroxyls, higher dispersion of Pt nanoparticles and higher adsorption capacity of AlOOH toward HCHO, and its larger specific surface area and pore volume. The in situ DRIFTS result indicated that the interaction of HCHO with surface oxygen resulted in the formation of formate, and then the oxidation of the formate to CO_2 and H_2O over Pt/AlOOH at room temperature. This study shows that the efficient catalysts for indoor air purification at room temperature, including for HCHO decomposition, can be designed by depositing nanoparticles of noble metals on mesoporous supports with abundance of surface hydroxyls and large surface area.

Acknowledgements

This work was partially supported by the 863 Program (2012AA062701), 973 Program (2013CB632402), NSFC (21307038, 51320105001, 51372190, 21177100 and 51272199), Key Project of Chinese Ministry of Education (212115), PSFC (2012M521482 and 2013T60754).

References

[1] Y. Sekine, A. Nishimura, Atmos. Environ. 35 (2001) 2001–2007.
[2] J.G. Yu, X.Y. Li, Z.H. Xu, W. Xiao, Environ. Sci. Technol. 47 (2013) 9928–9933.
[3] B.T. Liu, C.H. Hsieh, W.H. Wang, C.C. Huang, C.J. Huang, Chem. Eng. J. 232 (2013) 434–441.
[4] Z.H. Xu, J.G. Yu, G. Liu, Dalton Trans. 42 (2013) 10190–10197.
[5] Z.H. Xu, J.G. Yu, W. Xiao, Chem. Eur. J. 19 (2013) 9592–9598.
[6] B. Liu, Y. Liu, C. Li, W. Hu, P. Jing, Q. Wang, J. Zhang, Appl. Catal. B 127 (2012) 47–58.
[7] Z. Qu, S. Shen, D. Chen, Y. Wang, J. Mol. Catal. A 356 (2012) 171–177.
[8] P. Zhou, X. Zhu, J.G. Yu, W. Xiao, ACS Appl. Mater. Interfaces 5 (2013) 8165–8172.
[9] R. Akbarzadeh, S.B. Umbarkar, R.S. Sonawane, S. Takle, M.K. Dongare, Appl. Catal. A 374 (2010) 103–109.
[10] W. Liang, J. Li, Y. Jin, Build. Environ. 51 (2012) 345–350.
[11] L.H. Nie, J.G. Yu, X.Y. Li, B. Cheng, G. Liu, M. Jaroniec, Environ. Sci. Technol. 47 (2013) 2777–2783.
[12] H. Huang, D.Y.C. Leung, ACS Catal. 1 (2011) 348–354.
[13] C. Ma, D. Wang, W. Xue, B. Dou, H. Wang, Z. Hao, Environ. Sci. Technol. 45 (2011) 3628–3634.
[14] X. Yu, J. He, D. Wang, Y. Hu, H. Tian, Z. He, J. Phys. Chem. C 116 (2012) 851–860.
[15] N. An, Q. Yu, G. Liu, S. Li, M. Jia, W. Zhang, J. Hazard. Mater. 186 (2011) 1392–1397.
[16] L.H. Nie, A.Y. Meng, J.G. Yu, M. Jaroniec, Sci. Rep. 3 (2013) 3215.
[17] B. Chen, X. Zhu, M. Crocker, Y. Wang, C. Shi, Catal. Commun. 42 (2013) 93–97.
[18] H. Huang, D.Y.C. Leung, J. Catal. 280 (2011) 60–67.
[19] X. Lai, D. Wang, N. Han, J. Du, J. Li, C. Xing, Y. Chen, X. Li, Chem. Mater. 22 (2010) 3033–3042.
[20] H. Li, N. Zhang, P. Chen, M. Luo, J. Lu, Appl. Catal. B 110 (2011) 279–285.
[21] B. Chen, C. Shi, M. Crocker, Y. Wang, A. Zhu, Appl. Catal. B 132–133 (2013) 245–255.
[22] X. Tang, J. Chen, X. Huang, Y. Xu, W. Shen, Appl. Catal. B 81 (2008) 115–121.
[23] N. An, W. Zhang, X. Yuan, B. Pan, G. Liu, M. Jia, W. Yan, W. Zhang, Chem. Eng. J. 215–216 (2013) 1–6.
[24] I.I. Slowing, B.G. Trewyn, S. Giri, V.S.Y. Lin, Adv. Funct. Mater. 17 (2007) 1225–1236.
[25] M. Jaroniec, NATO Security through Science Series, 2006, pp. 23–36.
[26] Z. Wu, D. Zhao, Chem. Commun. 47 (2011) 3332–3338.
[27] A. Corma, Top. Catal. 4 (1997) 249–260.
[28] F. Chang, M. Zhang, G. Wang, W. Shi, X. Hu, Water Air Soil Pollut. 223 (2012) 2073–2081.
[29] T.H. Yoon, S.B. Johnson, G.E. Brown Jr., Langmuir 21 (2005) 5002–5012.
[30] P.F. Fulvio, R.I. Brosey, M. Jaroniec, ACS Appl. Mater. Interfaces 2 (2010) 588–593.
[31] X.X. Yu, J.G. Yu, B. Cheng, M. Jaroniec, J. Phys. Chem. C 113 (2009) 17527–17535.
[32] W.Q. Cai, J.G. Yu, S. Mann, Microporous Mesoporous Mater. 122 (2009) 42–47.
[33] Y. Feng, W. Lu, L. Zhang, X. Bao, B. Yue, Y. Lv, X. Shang, Cryst. Growth Des. 8 (2008) 41426–41429.
[34] J. Zhang, S. Wei, J. Lin, J. Luo, S. Liu, H. Song, E. Elawad, X. Ding, J. Gao, S. Qi, C. Tang, J. Phys. Chem. B 110 (2006) 21680–21683.
[35] H. Hou, Y. Xie, Q. Yang, Q. Guo, C. Tan, Nanotechnology 16 (2005) 741–745.
[36] W.Q. Cai, J.G. Yu, M. Jaroniec, J. Mater. Chem. 21 (2011) 9066–9072.
[37] W.Q. Cai, J.G. Yu, C. Anand, A. Vinu, M. Jaroniec, Chem. Mater. 23 (2011) 1147–1157.
[38] V. Vatanpour, S.S. Madaeni, L. Rajabi, S. Zinadini, A.A. Derakhshan, J. Membr. Sci. 401–402 (2012) 132–143.
[39] W.Q. Cai, J.G. Yu, B. Cheng, B.L. Su, M. Jaroniec, J. Phys. Chem. C 113 (2009) 14739–14746.
[40] Y. Wang, G. Wang, H. Wang, W. Cai, C. Liang, L. Zhang, Nanotechnology 20 (2009) 155604–155610.
[41] D. Chen, Z. Qu, S. Shen, X. Li, Y. Shi, Y. Wang, Q. Fu, J. Wu, Catal. Today 175 (2011) 338–345.
[42] Z.H. Xu, J.G. Yu, J.X. Low, M. Jaroniec, ACS Appl. Mater. Interfaces 6 (2014) 2111–2117.
[43] M. Jaroniec, L. Solovyov, Langmuir 22 (2006) 6757–6760.
[44] L. Zhang, Y. Zhu, J. Phys. Chem. C 112 (2008) 16764–16768.
[45] T.Z. Ren, Z.Y. Yuan, B.L. Su, Langmuir 20 (2004) 1531–1534.
[46] K.S.W. Sing, D.H. Everett, R.A.W. Haul, L. Moscou, R.A. Pierotti, J. Rouquerol, T. Siemieniewska, Pure Appl. Chem. 57 (1985) 603–619.
[47] C. Sangwichien, G.L. Aranovich, M.D. Donohue, Colloids Surf. A 206 (2002) 313–320.
[48] S.C. Shen, W.K. Ng, Z.Y. Zhong, Y.C. Dong, L. Chia, R.B.H. Tan, J. Am. Ceram. Soc. 92 (2009) 1311–1316.
[49] C. Gao, X.Y. Yu, R.X. Xu, J.H. Liu, X.J. Huang, ACS Appl. Mater. Interfaces 4 (2012) 4672–4682.
[50] X. Wang, H. Yu, D. Hua, S. Zhou, J. Phys. Chem. C 117 (2013) 7294–7302.
[51] J.T. Kloprogge, L.V. Duong, B.J. Wood, R.L. Frost, J. Colloid Interface Sci. 296 (2006) 572–576.
[52] A.M.A. Cruz, J.G. Eon, Appl. Catal. A 167 (1998) 203–213.
[53] C. Zhang, F. Liu, Y. Zhai, H. Ariga, N. Yi, Y. Liu, K. Asakura, M.F. Stephanopoulos, H. He, Angew. Chem. Int. Ed. 51 (2012) 9628–9632.
[54] J. Araña, C.G. Cabo, J.M. Doña-Rodríguez, O. González-Díaz, J.A. Herrera-Melián, J. Pérez-Peña, Appl. Surf. Sci. 239 (2004) 60–71.
[55] E.A. Ivanov, G.Y. Popova, Y.A. Chesalov, T.V. Andrushkevich, J. Mol. Catal. A 312 (2009) 92–96.
[56] C.B. Zhang, H. He, Catal. Today 126 (2007) 345–350.